Nickel-based catalysts for hydrogen evolution by hydrolysis of sodium borohydride: from structured nickel hydrazine nitrate complexes to reduced counterparts

Pierre Tignol, Umit Demirci

Nickel-based catalysts for hydrogen evolution by hydrolysis of sodium borohydride: from structured nickel hydrazine nitrate complexes to reduced counterparts

Pierre Tignol,[a,b] Umit B. Demirci [a,b,*]

[a] Institut Européen des Membranes, IEM – UMR 5635, CNRS, ENSCM, Univ Montpellier, Montpellier, France

[b] Départment de Chimie, Faculté des Sciences, Univ Montpellier, Montpellier, France

* Corr. author: umit.demirci@umontpellier.fr

Abstract

Nickel complexes have recently been presented as prospective catalytic materials for hydrogen H_2 evolution by hydrolysis of sodium borohydride $NaBH_4$. An attractive complex is nickel hydrazine nitrate $[Ni(N_2H_4)_3][NO_3]_2$ for which little variations in the synthesis procedure result in different morphologies like hexagonal plates, clews and discs. In our conditions, the clews have the better catalytic activity owing to more defects and more active sites. There is an effect of the morphology on the catalytic activity. However, the H_2 evolution curves (regardless the initial morphology) show an induction period during which the complex (purple violet in color) evolves into a catalytically active form (fine black powder). The evolution is featured by changes in morphology and chemical state of nickel. The catalytically active form is even more active than the pristine complex: it shows a higher H_2 generation rate (three times higher in the best case). The starting complexes and the "reduced" counterparts have been then characterized (*e.g.* SEM, FTIR, XRD, XPS) to better understand the aforementioned evolutions. One of our main conclusions is that there are some marked analogies between our nickel-based catalysts and the much-investigated cobalt-based catalysts.

Keywords

Hydrogen storage; Hydrolysis; Nickel; Mesostructure; Sodium borohydride.

1. Introduction

Hydrolysis of sodium borohydride $NaBH_4$ is a simple approach for the generation of high amounts of hydrogen H_2 at 10-80°C and under atmospheric pressure [1]:

$$NaBH_4\ (aq) + 4H_2O\ (l) \rightarrow NaB(OH)_4\ (aq) + 4H_2\quad (g) \qquad (1)$$

The attractive features of the reaction have been widely discussed in the open literature within the past two decades. One may cite three of them: half of the generated H_2 comes from water H_2O [2]; the couple $NaBH_4$-H_2O is able to achieve higher *effective* gravimetric hydrogen storage capacities (*e.g.* 6.5 wt%) than the other material-based solutions investigated so far for chemical H storage [3]; and, the H_2 generation rates are readily tuned by changing the catalyst and/or the operating conditions [4]. This however should not hide the fact that the reaction has also drawbacks, the main three being: the storage irreversibility implying a difficult regeneration of the spent fuel $NaB(OH)_4$ [5]; the recurring catalyst deactivation [6]; and the presence of borates in the H_2 stream [7]. Nonetheless hydrolysis of $NaBH_4$ has shown to still have real industrial and application prospects [8].

Accelerating the H_2 generation has been one of the most investigated aspects. Numerous homogenous and heterogeneous accelerators have been considered so far but the most prominent ones have been non-noble metal-based heterogeneous catalysts [4]. Cobalt is the leading catalytic metal. It is a promising option owing to low cost and high catalytic activity [9]. Yet its development is somehow hindered by the fact that it faces a recurring deactivation problem [6]. Another potential catalytic metal is nickel. The first works date back the first half of the 2000s. In 2003, Hua *et al.* reported a nickel boride Ni_xB catalyst being active for the release of H_2 at a rate of about 240 $mL(H_2)\ min^{-1}\ g_{NixB}^{-1}$ [10]. In 2004, Kim *et al.* described pasted filamentary nickel as an active catalyst that however gradually loses activity with cycling [11]. The catalytic activity degradation was explained by an agglomeration of the catalyst as well as the formation of a film on the pasted catalyst. The film was found to be mainly composed of borate species. Thereafter, a number of alternative nickel-based catalysts emerged. Examples are as follows: nickel (II) salts [12]; nickel nanoclusters [13]; bimetallic catalysts like NiRu [14]; trimetallic nanoparticles like NiAuCo [15]; nanocomposites with polymers [16] or silica [17]; and nickel nanoparticles supported on Fe_3O_4 [18] or on reduced graphene oxide-branched polyethyleneimine aerogel [19]. Recently new materials have been suggested as potential nickel-based catalysts. Kılınç *et al.* focused on coordination chemistry to propose a complex based on the interaction of the empty orbital of a nickel cation and the

lone pair electrons of ligands with nitrogen and oxygen atoms [**20**]. The nickel-5-amino-2,4-dichlorophenol-3,5-di-*tert*-butylsalisylaldehyde complex was prepared and used as catalysts in hydrolysis of $NaBH_4$. It was found to accelerate the reaction and then to retain 72% of its initial activity after a sixth use. Better performance in terms of activity and stability was afterwards achieved when the complex was supported on alumina [**21**].

Recently, we focused on the nickel hydrazine nitrate complex $[Ni(N_2H_4)_3][NO_3]_2$ (**Figure S1**). It is a coordination compound where the hexacoordinated metallic center is complexed by three N_2H_4 bidentate ligands. The overall charge of $[Ni(N_2H_4)_3]^{2+}$ is neutralized by two NO_3^- anions. Since 1997, it has been mainly considered for its energetic properties [**22-24**]. In the present work, the complex was considered as a potential catalyst for hydrolysis of $NaBH_4$. We had three scientific objectives: (*i*) synthesizing morphology-controlled complexes *via* a simple experimental procedure and studying the effect of the morphology on the catalytic activity; (*ii*) investigating the evolution of the morphology as well as that of the chemical state of nickel after the hydrolysis reaction, knowing that the reaction takes place in a reducing medium; (*iii*) and assessing the potential of such catalysts in terms of activity and stability (*i.e.* catalyst reusability) over cycles. Herein are presented our main results.

2. Experimental

The morphology-controlled nickel hydrazine nitrate complexes were prepared according to a procedure described elsewhere [**25**]. Three different morphologies were targeted (**Table S1**). Hexagonal plate-like morphology (denoted ***h*NHN**) was obtained at room conditions and as follows. In a 250-mL beaker, 0.17 g of nickel (II) nitrate hexahydrate ($Ni(NO_3)_2{\cdot}6H_2O$; Sigma-Aldrich) was weighted. 15.6 mL of an aqueous solution of polyvinylpyrrolidone (PVP; $(C_6H_9NO)_{360}$; 40000 g mol^{-1}; Sigma-Aldrich) at 1 mM was added under stirring, resulting in a green solution. Then, 2.1 mL of hydrazine hydrate ($N_2H_4{\cdot}H_2O$; 64-65 wt%, reagent grade 98%; Sigma-Aldrich) was added dropwise. After the first drop the solution turned blue. Upon the addition of hydrazine, the mixture was ultrasonicated for 15 min, resulting in the formation of a purple violet precipitate, in good agreement with the color of the nickel hydrazine nitrate complex (**Figure S2**) [**22-25**]. The solid was separated by centrifugation (6000 rpm; 10 min), the process being interspersed by two washings with deionized water (Millipore milli-Q, resistivity >18.2 MΩ cm) and one with ethanol. The solid was finally

dried at 60°C for 12 h. Clew-like morphology (denoted ***c*NHN**) was obtained according to a similar procedure except that two parameters changed. The volume of hydrazine hydrate was decreased to 0.52 mL and the ultrasonication time was increased to 1 h. With respect to the disc-like morphology (denoted ***d*NHN**), the PVP solution was substituted by an aqueous solution of polyethylene glycol (PEG; $H(OCH_2CH_2)_{90}OH$; 4000 g mol^{-1}; Sigma-Aldrich) at 1 mM; the volume of hydrazine hydrate was 0.52 mL; and the ultrasonication time was 15 min.

Visual inspection of the morphology-controlled nickel hydrazine nitrate complexes were carried out by optical microscopy (Leica ICC50W) and scanning electron microscopy (SEM; Hitachi S4800). Structural analyses were performed by Fourier-transform infrared spectroscopy (FTIR; Thermo Fisher Nexus; attenuated total reflection mode (ATR; DuraSamplIR); 4000-700 cm^{-1}; 32 scans), ^{11}B nuclear magnetic resonance (NMR; Bruker AVANCE-300; probe head BBO10 operated at 96.29 MHz; D_2O as reference), and ^{11}B magic angle spinning (MAS) NMR (Varian VNMR 400 spectrometer; 128.4 MHz). Crystallographic analyses were done by X-ray diffraction (XRD; PANalytical X'PERT Pro; Cu-Kα radiation λ = 1.5406 Å; working voltage 40 kV and working current 30 mA). For pattern matching, PANalytical X'Pert HighScore software and the available crystallographic databases (PDF-4+ v. 4.1403) were used. Surface analyses of the morphology-controlled nickel hydrazine nitrate complexes were performed by X-ray photoelectron spectroscopy (XPS; ESCALAB 250 from Thermo Electron; monochromatic source Al Kα ray 1486.6 eV; analyzed surface of 400 µm diameter; binding energies (BE) of all core levels referred to the C–C of C1s carbon at 284.8 eV). Thermal analyses of the hydrolysis by-product were carried out by thermogravimetric analysis (TGA; TA instruments Q500) and differential scanning calorimetry (DSC; TA Instruments Q20). For both techniques, ~10 mg of sample was analyzed under the following conditions: 25-400°C, heating rate of 5 ºC min^{-1}, and N_2 flow of 60 mL min^{-1}.

The hydrolysis experiments were performed on our catalytic set-up based on the inverted-burette method. It is made up of a reactor (Schlenk-type tube), a cold trap, and an inverted burette filled with blue-colored water. In the present work, the hydrolysis conditions were as follows: 80°C; 11 mg of catalyst (10 wt% of the couple catalyst-borohydride); 2 mL of an aqueous alkaline (NaOH at 0.5 M) solution of $NaBH_4$ (100 mg, corresponding to 90 wt% of the couple catalyst-borohydride). The molar ratio $H_2O/NaBH_4$ was 42, implying an excess of water in relation to the stoichiometric reaction shown by Eq. 1. Lower temperatures were

applied for the determination of the apparent activation energies with the help of the Arrhenius equation. The variation of the volume of H_2 was systematically video-recorded to be computationally exploited and to plot the time-dependent H_2 evolution curve. The H_2 generation rate was determined over the linear part of the H_2 evolution curve (*i.e.* slope of the curves).

3. Results and discussion

3.1. Characterization of the complexes

The nickel hydrazine nitrate (denoted also **NHN**) complexes were targeted in three morphologies: hexagonal plates, clew-like objects, and discs. They are denoted ***h*NHN**, ***c*NHN** and ***d*NHN** respectively. The successful synthesis of each of these morphologies was first visually verified by optical microscopy (**Figure S3**). The presence of hexagonal plates and discs are confirmed for ***h*NHN** and ***d*NHN**. Spherical shapes similar to clew-like morphologies can be seen for ***c*NHN**. A precise observation was performed by SEM (**Figure 1**). ***h*NHN** mainly consists of hexagonal plate-like objects of about 3 µm. Clew-like morphologies of equivalent size are also seen. With ***c*NHN**, shapes that can be compared to clews were observed. They are big, with sizes of 6-7 µm. However there are other objects of smaller size and of different shapes. The SEM image of ***d*NHN** shows a binary mixture of discs and clew-like morphologies. The mixture is homogeneous in terms of size, with an average of 2 µm. Our observations are in quite good agreement with those reported in the seminal work [**25**].

The samples ***h*NHN**, ***c*NHN** and ***d*NHN** were analyzed by FTIR spectroscopy (**Figure 2**). The spectra are identical for the three morphologies. They show bands in the stretching and deformation regions of both of the N–H and N–O bonds [**24**,**26**-**28**]. The spectra were also compared to the spectrum of another nickel hydrazine complex, *i.e.* $[Ni(N_2H_4)_3][Cl]_2$ [**29**]. Parallels were found for the N–H and N–N vibrational bands. Our spectroscopic observations are in accordance with the formation of the complex $[Ni(N_2H_4)_3][NO_3]_2$.

The XRD patterns (**Figure S4**) are identical for ***h*NHN**, ***c*NHN** and ***d*NHN**. They match the pattern of $[Ni(N_2H_4)_3][NO_3]_2$ reported elsewhere [**30**] where it revealed a trigonal structure, with a space group *P-3c1*.

XPS analyses were performed and similar spectra were obtained for ***h*NHN**, ***c*NHN** and ***d*NHN** (**Figure S5**). The binding energies (BE) were ascribed with the help of the NIST XPS database [**31**]. For Ni 2p1/2 (*e.g.* 873.6 eV for ***h*NHN**) and Ni 2p3/2 (*e.g.* 855.9 eV for ***h*NHN**), the BEs (**Figure 3**) are consistent with values reported for Ni^{2+} (in *e.g.* complexes). For N 1s, there are two signals, at 400.1-400.3 eV and 406.3-406.8 eV (**Figure 4**). They may be respectively attributed to amine/hydrazine and nitrate groups found in metal complexes. The XPS data are thus in good agreement with the molecular structure $[Ni(N_2H_4)_3][NO_3]_2$.

3.2. Catalytic activity of the complexes

The catalytic activity of ***h*NHN**, ***c*NHN** and ***d*NHN** was assessed for the generation of H_2 by hydrolysis of $NaBH_4$ at 80°C. The H_2 evolution curves are shown in **Figure 5**. They look sigmoidal and the curve can be divided into three parts.

The first part corresponds to the first minutes of the reaction during which the H_2 evolution gradually increases. It resembles to the induction period generally reported for cobalt-based catalysts [**6**,**9**]: during this period, the catalyst surface is transformed (often reduced) into a catalytically active form.

The second part of the curves is the linear part. It is due to the proper hydrolysis of $NaBH_4$ [**32**], where the H_2 generation rate is constant. It is calculated to be 10.2, 14.2 and 17 $mL(H_2)$ min^{-1} for ***h*NHN**, ***d*NHN** and ***c*NHN** respectively. Expressed in $L(H_2)$ min^{-1} g_{NHN}^{-1}, the rates are 0.93, 1.29 and 1.55 respectively. The better catalytic activity of ***c*NHN** is explained by a higher number of active sites owing to more surface defects (**Figure 1**). With respect to ***d*NHN**, it is more active than ***h*NHN**. This can be due to the presence of clew-like particles (**Figure 1**). In comparison to previously reported catalysts [**4**], the catalytic activity of ***h*NHN**, ***c*NHN** and ***d*NHN** is average. With respect to the salisylaldimine-nickel complex reported by Kılınç *et al.* [**20**], a rate of 2.24 $L(H_2)$ min^{-1} $g_{complex}^{-1}$ was found at 30°C, such a performance being explained by the relatively high specific surface area of 48.5 m^2 g^{-1}; the rate was even improved by a factor of 28 by supporting the complex onto alumina [**21**].

The third part of the H_2 evolution curves is characterized by rates dropping to 0 $mL(H_2)$ min^{-1} because of the depletion of $NaBH_4$ in the slurry (end of the reaction).

In order to calculate the apparent activation energy, the temperature of the hydrolysis experiment was varied from 50 to 80°C. Predictably, the H_2 generation rates (determined *via* the linear part of the curves) were found to drop with the decrease of the temperature (**Figures S6** to **S8**). They were injected in the Arrhenius equation to plot their Napierian logarithm as a function of the reverse of the temperature in Kelvin (**Figure S9**). The slope of the as-obtained line was multiplied by R = 8.314 J mol^{-1} K^{-1} to get the apparent activation energy, namely, 38.7 ± 5, 48.7 ± 4 and 49.5 ± 4 kJ mol^{-1} for ***h*NHN**, ***c*NHN** and ***d*NHN** respectively. They are consistent with most of the values reported for metal-catalyzed hydrolysis of $NaBH_4$ [**33**].

After hydrolysis, the spent fuel was recovered for analyses (**Figure 6**). The liquid-state spent fuel was first analyzed by NMR of the nucleus ^{11}B. There is no signal at negative shifts, indicating a total hydrolysis of $NaBH_4$. One singlet is viewed at 2.55 ppm. It is typical of the tetrahydroxyborate anion $B(OH)_4^-$ [**34**]. The water of the liquid-state spent fuel was extracted at 60°C for 72 h and the as-obtained solid spent fuel was kept at this temperature. It was analyzed by ^{11}B MAS NMR. There is only one signal peaking at 2.04 ppm. This is in good agreement with tetravalent B found in boron oxides and borates like $NaB(OH)_4$ [**35**]. The fingerprint of a borate like $NaB(OH)_4$ was obtained by FTIR spectroscopy [**36**]. Another evidence of the formation of $NaB(OH)_4$ is the XRD pattern. It well matches the reference pattern 01-081-1512 (score of 78) that suggests a crystalline $NaB(OH)_4$ compound with a monoclinic structure and the space group *P21/a*. A last confirmation of the nature of the borate (also denoted $NaBO_2{\cdot}2H_2O$) comes from the TGA and DSC results (**Figure S10**). It is observed a stepwise evolution from 100°C to 400°C that may be attributed to H_2O desorption [**37**]. The weight loss at 400°C is 34.2 wt% while the water content in $NaB(OH)_4$ is 35.3 wt%. Over this temperature range, $NaBO_2{\cdot}2H_2O$ loses two equivalents of H_2O, much likely resulting in the formation of sodium metaborate $NaBO_2$.

Prior to any analysis, the aforementioned liquid-state spent fuel was first separated from the catalyst by centrifugation (6000 rpm for 10 min). We systematically observed that, during the hydrolysis experiments, the solids changed color from purple violet to black (**Figure S2**), indicating the occurrence of a transformation as also suggested by the occurrence of an induction period (**Figure 5**) [**6**,**9**]. Similar color change upon reduction was observed for the

complex $[Ni(N_2H_4)_3][Cl]_2$ [29]. The black solids were washed with water twice, with ethanol once, and dried at 80°C overnight. For each solid, a fine powder was recovered for analyses.

3.3. Characterization of the black "reduced" complexes

The complexes after hydrolysis were supposed to be "reduced" [6,9] because of the reducing character of $NaBH_4$. Accordingly the "reduced" counterparts of ***h*NHN**, ***c*NHN** and ***d*NHN** (*i.e.* after hydrolysis) are denoted **R*h*NHN**, **R*c*NHN** and **R*d*NHN** (with R for reduced).

The fine powders **R*h*NHN**, **R*c*NHN** and **R*d*NHN** were scrutinized by optical microscopy. The initial morphologies were not found (**Figure S11**). They were then observed by SEM (**Figure 7**). Each of the complexes evolved from a morphological point of view. Spherical particles are observed for **R*h*NHN**, **R*c*NHN** and **R*d*NHN**. There are however few differences. The spherical shape is not perfect with **R*h*NHN** and the particles (with an average size of 120 nm) are much agglomerated (**Figure S12**). One may even distinguish the presence of very few hexagonal plates (**Figure S13**) and which surface is much rougher than for ***h*NHN**. With respect to **R*c*NHN**, the particles are spherical and agglomerated (**Figure S14**). Their size is quite uniform with 100 nm. The sample **R*d*NHN** has a more heterogeneous composition, with spherical particles of 120-160 nm as well as clew-like morphologies (**Figure S15**). They look like the spherical particles of 150-180 nm reported elsewhere and that they were found to form from the complex $[Ni(N_2H_4)_3][Cl]_2$ by hydrazine reduction [29,38].

The samples **R*h*NHN**, **R*c*NHN** and **R*d*NHN** were analyzed by FTIR spectroscopy (**Figure S16**). The spectra are comparable for the three compounds, but they are much different from the spectra collected with the starting complexes (**Figure 2**). These results are in accordance with an evolution of the complexes. The bands are wider and for most they do not have the same wavenumber. The observed vibrational bands were favorably compared to the bands generally reported for borate species [26,36,37]. The presence of hydrazine cannot be discarded [24,26-29], at least for **R*d*NHN**. The spectra over the wavenumber range 3600-1600 cm^{-1} resemble the one reported for the complex $[Ni(N_2H_4)_3][Cl]_2$ after reduction by hydrazine [29]; in that study, the formation of $Ni(OH)_2$ was evidenced.

The samples **R*h*NHN**, **R*c*NHN** and **R*d*NHN** were analyzed by XRD (**Figure S17**). They did not diffract, suggesting amorphous solids. Similar observations were made for various cobalt-based catalysts or precursors of *in situ* forming catalysts; upon reduction by $NaBH_4$, cobalt was found to be amorphous, resulting in a debate about the nature of the catalytically active phase [**9**,**39**]. Here, the XRD patterns of **R*h*NHN**, **R*c*NHN** and **R*d*NHN** (**Figure S17**) display one broad shoulder of low intensity at about 2θ 45°. In comparison to the most intense diffraction peak that can be observed in the referenced pattern of various nickel-based compounds, several species might be suggested. Examples are cubic nickel (ref. 00-004-0850), tetragonal Ni_2B (ref. 00-048-1222), orthorhombic Ni_3B (00-048-1223), and cubic NiO (ref. 00047-1049). A further discussion at this point would be, as for the aforementioned cobalt-based catalysts, speculative.

The samples **R*h*NHN**, **R*c*NHN** and **R*d*NHN** were then analyzed by XPS (**Figure S18**). The binding energies (BE) were ascribed with the help of the NIST XPS database [**31**]. The BEs measured for Ni 2p (**Figure 8**) are much comparable to the values reported for the fresh samples (**Figure 3**), suggesting Ni^{2+}-based surfaces. The formation of nickel hydroxide $Ni(OH)_2$ cannot be discarded [**29**]. Boron was found on the superficial layers of **R*h*NHN**, **R*c*NHN** and **R*d*NHN** (**Figure 9**). The B 1s BE is 191.8 ± 0.1 eV. This is a typical value for borates and other boron oxides. No nitrogen was detected on the surface of both **R*h*NHN** and **R*c*NHN**. One N 1s signal was distinguished for **R*d*NHN** (**Figure S19**). The BE of is 399.7 eV indicating the presence of residual hydrazine groups. According to the XPS results, the surface of the spherical particles observed for **R*h*NHN**, **R*c*NHN** and **R*d*NHN** are composed of Ni^{2+} and borate species. It is worth mentioning that similar observations for *in situ* forming cobalt-based catalysts were interpreted as the formation of surface species of formulae $Co^{II}@B_xO_y(OH)_z$ [**9**,**39**]. In the present conditions, the formation of surface $Ni^{II}@B_xO_y(OH)_z$ might be assumed.

3.4. Catalytic activity of the black "reduced" complexes

R*h*NHN, **R*c*NHN** and **R*d*NHN** were tested for their catalytic ability in hydrolysis of $NaBH_4$ (**Figures S20** to **S22**). They were compared to ***h*NHN**, ***c*NHN** and ***d*NHN** respectively. The results are summarized in **Figure 10**, where the cycle 0 refers to the H_2 generation rates of ***h*NHN**, ***c*NHN** and ***d*NHN** and the cycle 1 refers to H_2 generation rates of **R*h*NHN**, **R*c*NHN** and **R*d*NHN**. Two observations stand out. First, the reduced forms of the complexes are more

active than the fresh counterparts. For example, the H_2 generation rate of **R*h*NHN** is almost thrice the H_2 generation rate of ***h*NHN**. The explanation of that may be the smaller size of the particles observed for **R*h*NHN**, **R*c*NHN** and **R*d*NHN** (**Figure 7** *vs.* **Figure 1**). Second, the H_2 evolution curves of **R*h*NHN**, **R*c*NHN** and **R*d*NHN** does not show an induction period. This is typical of a catalyst which surface consisted of the catalytically active sites [**6**,**9**]. This confirms that the surface of ***h*NHN**, ***c*NHN** and ***d*NHN** evolved during the cycle 0 into the active form found for **R*h*NHN**, **R*c*NHN** and **R*d*NHN**.

When the catalytic activities of **R*h*NHN**, **R*c*NHN** and **R*d*NHN** are compared to each other (**Figure 10**), it stands out that the H_2 generation rates are comparable: 28.7 mL(H_2) min^{-1} for **R*h*NHN**, 28.8 mL(H_2) min^{-1} for **R*c*NHN**, and 29.4 mL(H_2) min^{-1} for **R*d*NHN**. Expressed in L(H_2) min^{-1} g_{NHN}^{-1}, the rates are between 2.6 and 2.7 respectively. This is consistent with the microcopy observations (**Figure 7**) and the performed characterizations (**Figures 8** and **9**); indeed there is almost no difference between the three samples **R*h*NHN**, **R*c*NHN** and **R*d*NHN**. In other words, the initial morphology of ***h*NHN**, ***c*NHN** and ***d*NHN** does not have a remarkable impact on the morphology, structure and catalytic activity of **R*h*NHN**, **R*c*NHN** and **R*d*NHN**. Note that the aforementioned rates are slightly better than the rate (2.24 L(H_2) min^{-1} $g_{complex}^{-1}$) reported for another nickel complex [**20**].

Reusability tests were carried out with **R*h*NHN**, **R*c*NHN** and **R*d*NHN** (**Figure 10**). The cycle 2 to the cycle 5 refer to successive uses of these samples. After each cycle, the catalyst was extracted from the reaction slurry by centrifugation, washed twice with water, washed once with ethanol and dried at 80°C to be re-used. The reusability tests show a decrease of the H_2 generation rates, specifically of 19-28% at the cycle 2 and of 43-47% at the cycle 5 when the rates are compared to those of the cycle 1. In our conditions, these “reduced” catalysts deactivate over cycles. They behave as the *in situ* forming cobalt-based catalysts do [**9**,**39**] and, similarly, poisoning due to strong borates adsorption is much likely [**11**].

The apparent activation energy for each of the samples **R*h*NHN**, **R*c*NHN** and **R*d*NHN** was determined (**Figures S23** to **S26**). It was found: 48.1 ± 5, 50.3 ± 5 and 41.6 ± 5 kJ mol^{-1} respectively. They are comparable to the energies found for the fresh complexes. They are besides consistent with most of the values reported for metal-catalyzed hydrolysis of $NaBH_4$ [**33**].

3.5. Putting in perspective

Nickel complexes have been recently proposed as being potential catalysts for the evolution of H_2 by hydrolysis of $NaBH_4$ [**20**,**21**]. Our first objective was thus to gain more insight. Considering besides that the morphology of nickel complexes can be quite easily controlled by tuning the synthesis conditions [**25**], the objective was expanded to the study of the effect of the morphology on the catalytic activity of the samples. Three morphologies (hexagonal plate-like, clew-like and disc-like) of the nickel hydrazine nitrate complex were successfully targeted. They showed slightly different catalytic performances. All of them allowed getting a total conversion of $NaBH_4$ into H_2 and $NaB(OH)_4$, but this was achieved at different H_2 generation rates. The most efficient complex was found to be the clew-like morphology because it has more defects (particularly *via* the numerous edges and corners it has); this means more active sites.

The aqueous alkaline solution of $NaBH_4$ is reductive [**1**-**4**]. With metal cations used as precursors of *in situ*-forming catalysts, the evolution takes place during the first seconds/minutes of the reaction during the so-called induction period [**6**,**9**,**39**]. An induction period was observed with our nickel hydrazine nitrate complexes, suggesting an evolution towards a catalytically active form. The first evidence was a change of the color of the powder (from purple violet to black). The second evidence was provided by a set of characterization results. The nature of the "reduced" samples is not identified yet. Like for the much-investigated cobalt [**9**,**39**], the results are difficult to exploit and are open to speculation. Like for some of the cobalt-based catalysts, it was tentatively suggested the formation of surface $M^{II}@B_xO_y(OH)_z$ (with M = Ni or Co). The evolution of the nickel hydrazine nitrate complexes during the hydrolysis reaction has two additional consequences. Morphologically, the samples change towards aggregated spherical particles of much smaller size (100-160 nm). Catalytically, the "reduced" samples are more active in hydrolysis. The H_2 generation rates were found to be, at best, thrice of the rates determined with the fresh complexes. It may be concluded that the fresh nickel hydrazine nitrate complexes are not appropriate as catalysts for the hydrolysis of $NaBH_4$. In contrast, they may be seen as precursors of catalytic fine powders since the "reduced" forms have better catalytic potential.

Unless the catalyst is intended to be used once (one-shot approach) [**1**], it is important to assess the stability (or reusability) of the catalyst over cycles. This was our third objective. The nickel hydrazine nitrate complex evolves in a form that is more efficient. This "reduced" form was thus re-used in five cycles. The H_2 generation rates were found to decrease cycle after cycle. At best, 57% of the initial catalytic activity was retained after the fifth cycles. However, the total conversion of $NaBH_4$ was not affected, being constant at 100%. These results are also comparable to what was reported for cobalt-based catalysts so far [**1**,**4**,**6**,**9**,**39**]. It may be concluded that the active surface of *in situ*-forming Ni^{2+}- and Co^{2+}-based catalysts have more than one common feature.

4. Conclusion

Morphology-controlled nickel complexes are possible catalytic accelerators for H_2 evolution by hydrolysis of $NaBH_4$. In the present work, the nickel hydrazine nitrate complex $[Ni(N_2H_4)_3][NO_3]_2$ has been studied as microscale hexagonal plate-, clew- and disc-like structures. They are indeed able to catalyze the hydrolysis of $NaBH_4$, with H_2 generation rates being in the average of what has been reported hitherto in the field.

The clew-like sample is more active owing to more defects and more active sites. The H_2 evolution curves however show an induction period that suggests an evolution of the complex. A catalytically active material (called "reduced" sample) forms and this has been confirmed by visual inspection as well as by characterizations. The main observations are as follows. The color of the solids changes from purple violet to black. SEM observations of the as-obtained fine black powders reveal a change in the morphology; whatever the initial shape of the complex, aggregated nanoscale spherical particles (100-160 nm) form. The XRD pattern shows the transition from a crystalline material (trigonal, space group *P-3c1*) to an amorphous compound. According to the XPS scans, the nickel element still has an oxidation state of +2 but the hydrazine ligand and the nitrate anion have been mostly removed; instead boron is found.

Such observations are alike what has been reported and debated at length for Co^{2+} within the past decade. By analogy, it is tentatively suggested that Ni^{2+} and Co^{2+} behave in a similar way and that surface species such as $M^{II}@B_xO_y(OH)_z$ (with M = Ni or Co) might form. In our

conditions, the “reduced” sample is more active for H_2 evolution by hydrolysis of $NaBH_4$. In the best case, the H_2 generation rate is increased threefold, making it more attractive than the starting complex. Reusability tests performed with the “reduced” sample shows that the total conversion of $NaBH_4$ is constant but the H_2 generation rates drop cycle after cycle. More than 50% of the initial catalytic activity is retained after the fifth cycles. This result also makes our *in situ*-forming Ni^{2+}-based black fine powder resemble the *in situ*-forming Co^{2+}-based black solid.

In closing, there are opportunities for the nickel-based complexes as catalysts and/or catalyst precursors for hydrolysis of $NaBH_4$. Using nickel makes sense as it is much cheaper than cobalt.

Acknowledgements

The authors thank Maria-José Valero-Pedraza (Univ Montpellier) and Salem Ould-Amara (Univ Montpellier) for occasional assistance in XRD and NMR.

References

[1] Demirci UB. About the technological readiness of the H_2 generation by hydrolysis of B(−N)−H compounds. Energy Technol 2018;6:470–86.

[2] Schlesinger HI, Brown HC, Finholt AE, Gilbreath JR, Hoekstra HR, Hyde EK. Sodium borohydride, its hydrolysis and its use as a reducing agent and in the generation of hydrogen. J Am Chem Soc 195;75:215–9.

[3] Gislon P, Monteleone G, Prosini PP. Hydrogen production from solid sodium borohydride. Int J Hydrogen Energy 2009;34:929–37.

[4] Brack P, Dann SE, Wijayantha KGU. Heterogeneous and homogenous catalysts for hydrogen generation by hydrolysis of aqueous sodium borohydride ($NaBH_4$) solutions. Energy Sci Eng 2015;3:174–88.

[5] Liu CH, Chen BH. The concept about the regeneration of spent borohydrides and used catalysts from green electricity. Materials 2015;8:3456–66.

[6] Arzac GM, Hufschmidt D, Jiménez De Haro MC, Fernández A, Sarmiento B, Jiménez MA, Jiménez MM. Deactivation, reactivation and memory effect on Co–B catalyst for sodium borohydride hydrolysis operating in high conversion conditions. Int J Hydrogen Energy 2012;37:14373–81

[7] Petit E, Miele P, Demirci UB. By-product carrying humidified hydrogen: an underestimated issue in the field of hydrolysis of sodium borohydride $NaBH_4$. Chem Sus Chem 2016;9:1777–81.

[8] Lapeña-Rey N, Blanco JA, Ferreyra E, Lemus JL, Pereira S, Serrot E. A fuel cell powered unmanned aerial vehicle for low altitude surveillance missions. Int J Hydrogen Energy 2017;42:6926–40.

[9] Patel N, Miotello A. Progress in Co–B related catalyst for hydrogen production by hydrolysis of boron-hydrides: a review and the perspectives to substitute noble metals. Int J Hydrogen Energy 2015;40:1429–64.

[10] Hua D, Hanxi Y, Xinping A, Chuansin C. Hydrogen production from catalytic hydrolysis of sodium borohydride solution using nickel boride catalyst. Int J Hydrogen Energy 2003;28:1095–100.

[11] Kim JH, Kim KT, Kang YM, Kim HS, Song MS, Lee YJ, Lee PS, Lee JY. Study on degradation of filamentary Ni catalyst on hydrolysis of sodium borohydride. J Alloys Compd 2004;379:222–7.

[12] Cento C, Gislon P, Prosini PP. Hydrogen generation by hydrolysis of $NaBH_4$. Int J Hydrogen Energy 2009;34:4551–4.

[13] Metin Ö, Özkar S. Hydrogen generation from the hydrolysis of sodium borohydride by using water dispersible, hydrogenphosphate-stabilized nickel(0) nanoclusters as catalyst. Int J Hydrogen Energy 2007;32:1707–15.

[14] Ferreira MJF, Gales L, Fernandes VR, Rangel CM, Pinto AMFR. Alkali free hydrolysis of sodium borohydride for hydrogen generation under pressure. Int J Hydrogen Energy 2010;35:9869–78.

[15] Jiao C, Huang Z, Wang X, Zhang H, Lu L, Zhang S. Synthesis of Ni/Au/Co trimetallic nanoparticles and their catalytic activity for hydrogen generation from alkaline sodium borohydride aqueous solution. RSC Adv 2015;5:34364–71.

[16] Cai H, Lu P, Dong J. Robust nickel–polymer nanocomposite particles for hydrogen generation from sodium borohydride. Fuel 2016;166:297–301.

[17] Umegaki T, Hui SZ, Kojima Y. Fabrication of hollow silica–nickel particles for the hydrolytic dehydrogenation of ammonia borane using rape pollen templates. New J Chem 2017;41:992–6.

[18] Miao L, Zhu YZ, Wang HF. Nickel-decorated Fe_3O_4 nanoparticles as recyclable magnetic self-stirring nanocatalysts for microreactions. ACS Sust Chem Eng 2017;5:1864–70.

[19] Nabid MR, Bide Y, Dastar F. One pot synthesis of nickel nanoparticles stabilized on rGO/polyethyleneimine aerogel for the catalytic hydrogen generation. Catal Lett 2015;145:1798–807.

[20] Kılınç D, Şahin Ö, Saka C. Investigation on salisylaldimine-Ni complex catalyst as an alternative to increasing the performance of catalytic hydrolysis of sodium borohydride. Int J Hydrogen Energy 2017;42:20625–37.

[21] Kılınç D, Şahin Ö, Saka C. Salisylaldimine-Ni complex supported on Al_2O_3: highly efficient catalyst for hydrogen production from hydrolysis of sodium borohydride. Int J Hydrogen Energy 2018;43:251–61.

[22] Zhu S, Wu Y, Zhang W, Mu J. Evaluation of a new primary explosive: nickel hydrazine nitrate (NHN) complex. Propellants Explos Pyrotech 1997;22:314–20.

[23] Hariharanath B, Chandrabhanu KS, Rajendran AG, Ravindran M, Kartha CB. Detonator using nickel hydrazine nitrate as primary explosive. Def Sci J 2006;56:383–9.

[24] Wojewódka A, Bełzowski J. Hydrazine complexes of transition metals as perspective explosives. Chemik 2011;65:20–7.

[25] Wang Q, Geng B, Wang S, Liu J, Cheng Z, Si D. A facile sonochemical route to morphology controlled nickel complex mesostructures. Cryst Eng Comm 2009;11:1317–22.

[26] Miller FA, Wilkins CH. Infrared spectra and characteristic frequencies of inorganic ions. Anal Chem 1952;24:1253–94.

[27] Patil KC, Nesamani C, Verneker VRP. Synthesis and characterisation of metal hydrazine nitrate, azide and perchlorate complexes. Synth React Inorg Met Org Chem 1982;12:383–95.

[28] Chhabra JS, Talawar MB, Makashir PS, Asthana SN, Singh H. Synthesis, characterization and thermal studies of (Ni/Co) metal salts of hydrazine: potential initiatory compounds. J Hazard Mater 2003:A99;222–39.

[29] Park JW, Chae EH, Kim SH, Lee JH, Kim JW, Yoon SM, Choi JY. Preparation of fine Ni powders from nickel hydrazine complex. Mater Chem Phys 2006;97:371–8.

[30] Bushuyev OS, Brown P, Maiti A, Gee RH, Peterson GR, Weeks BL, Hope-Weeks LJ. Ionic polymers as a new structural motif for high-energy-density materials. J Am Chem Soc 2012;134:1422–5.

[31] NIST X-ray Photoelectron Spectroscopy Database. http://srdata.nist.gov/xps/, 2012. (accessed 15.07.18).

[32] Garron A, Swierczynski D, Bennici B, Auroux A. New insights into the mechanism of H_2 generation through $NaBH_4$ hydrolysis on Co-based nanocatalysts studied by differential reaction calorimetry. Int J Hydrogen Energy 2009;34:1185–99.

[33] Retnamma R, Novais AQ, Rangel CM. Kinetics of hydrolysis of sodium borohydride for hydrogen production in fuel cell applications: A review. Int J Hydrogen Energy 2011;36:9772–90.

[34] Sinton SW. Complexation chemistry of sodium borate with poly(vinyl alcohol) and small diols. A ^{11}B NMR study. Macromolecules 1987;20:2430–41.

[35] Zhou B, Sun Z, Yao Y, Pan Y. Correlations between ^{11}B NMR parameters and structural characters in borate and borosilicate minerals investigated by high-resolution MAS NMR and ab initio calculations. Phys Chem Minerals 2012;39:363–72.

[36] Jun L, Shuping X, Shiyang G. FT-IR and Raman spectroscopic study of hydrated borates. Spectrochim Acta 1995;51A:519–32.

[37] Kanturk A, Sari M, Piskin S. Synthesis, crystal structure and dehydration kinetics of $NaB(OH)_4 \cdot 2H_2O$. Korean J Chem Eng 2008;25:1331–7.

[38] Huang GY, Xu SM, Xu G, Li LY, Zhang LF. Preparation of fine nickel powders via reduction of nickel hydrazine complex precursors. Trans Nonferrous Met Soc China 2009;19:389–93.

[39] Demirci UB, Miele P. Cobalt-based catalysts in hydrolysis of $NaBH_4$ and NH_3BH_3. Phys Chem Chem Phys 2014;16:6872–85.

Figure 1. SEM images of the nickel hydrazine nitrate complexes denoted ***h*NHN** (hexagonal plate-like morphology), ***c*NHN** (clew-like morphology) and ***d*NHN** (disc-like morphology).

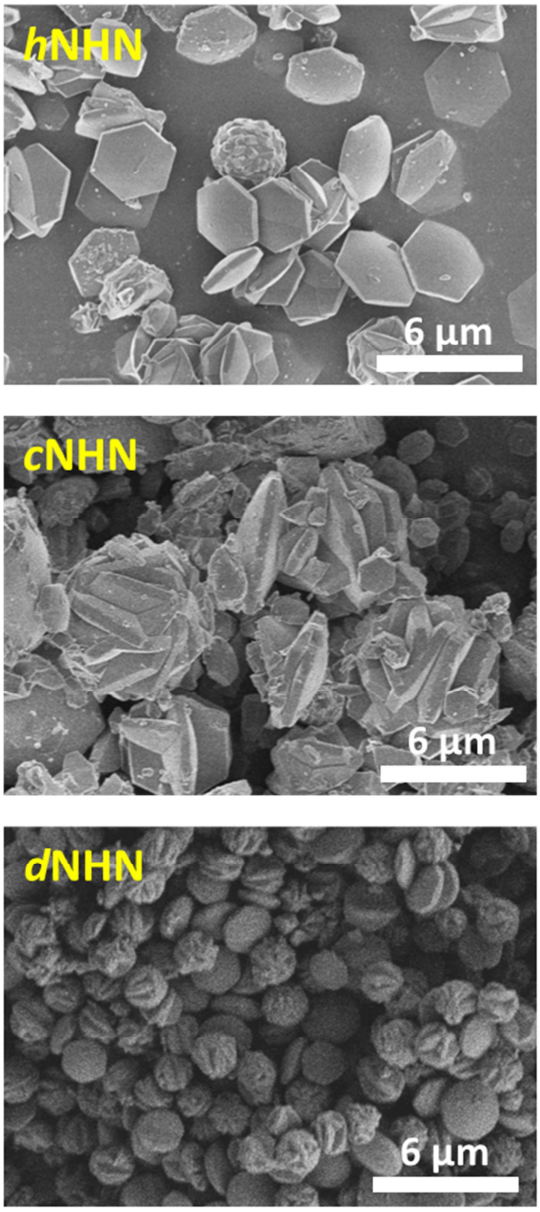

Figure 2. FTIR spectra of the nickel hydrazine nitrate complexes denoted ***h*NHN** (hexagonal plate-like morphology), ***c*NHN** (clew-like morphology) and ***d*NHN** (disc-like morphology).

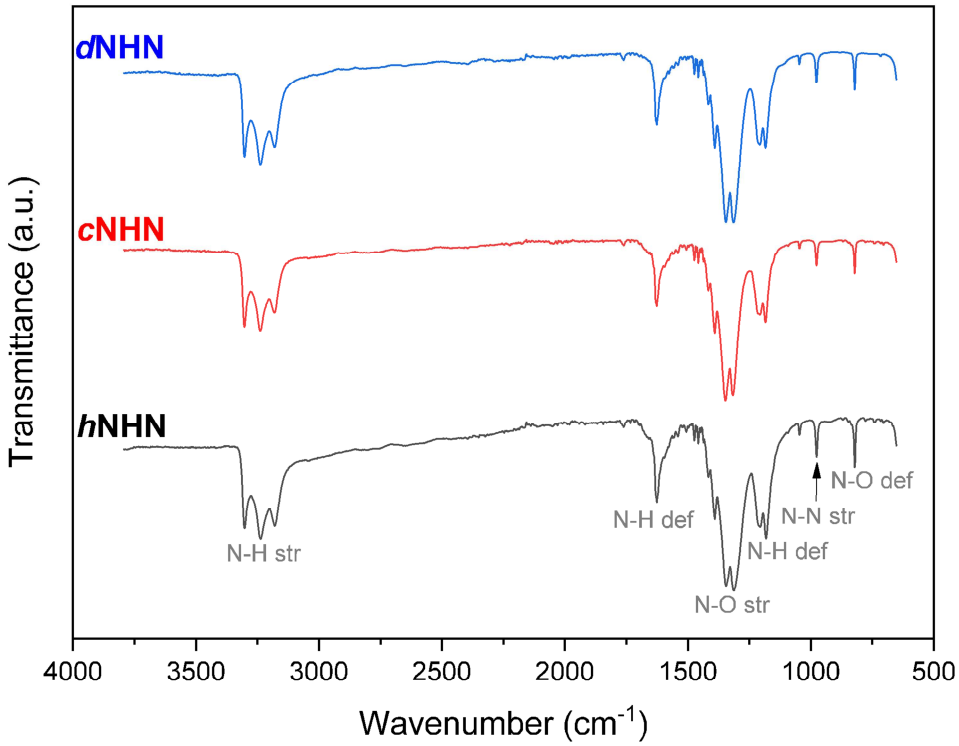

Figure 3. XPS spectra of the nickel hydrazine nitrate complexes denoted ***h*NHN** (hexagonal plate-like morphology), ***c*NHN** (clew-like morphology) and ***d*NHN** (disc-like morphology): focus on the Ni 2p signals.

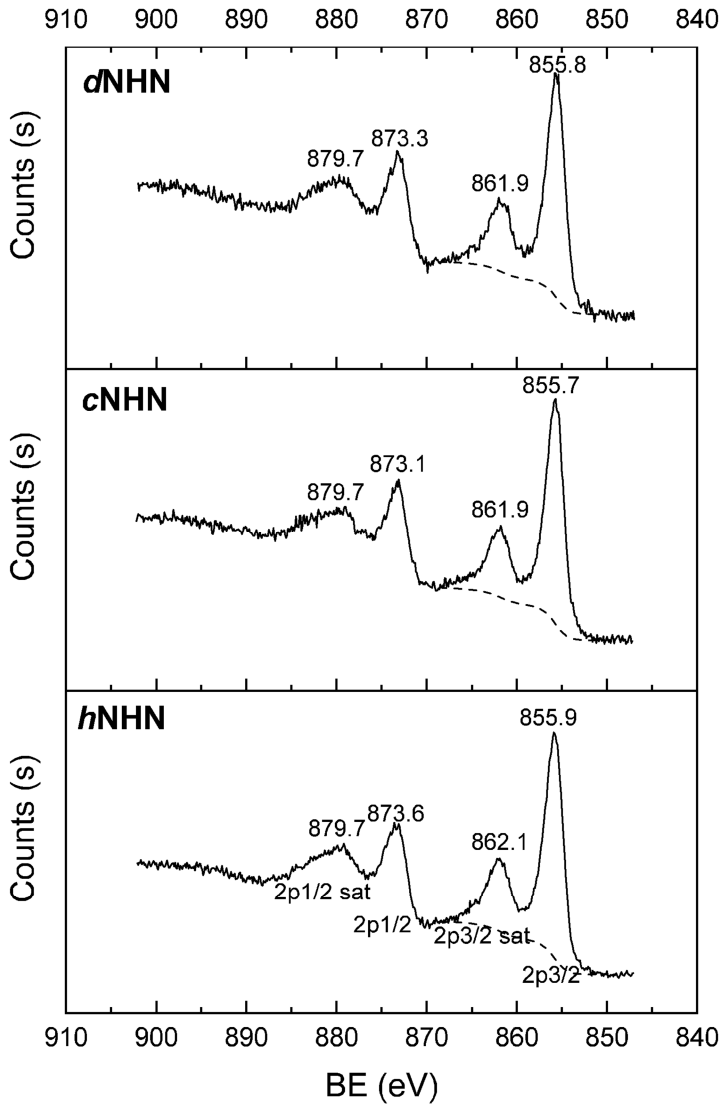

Figure 4. XPS spectra of the nickel hydrazine nitrate complexes denoted ***h*NHN** (hexagonal plate-like morphology), ***c*NHN** (clew-like morphology) and ***d*NHN** (disc-like morphology): focus on the N 1s signals.

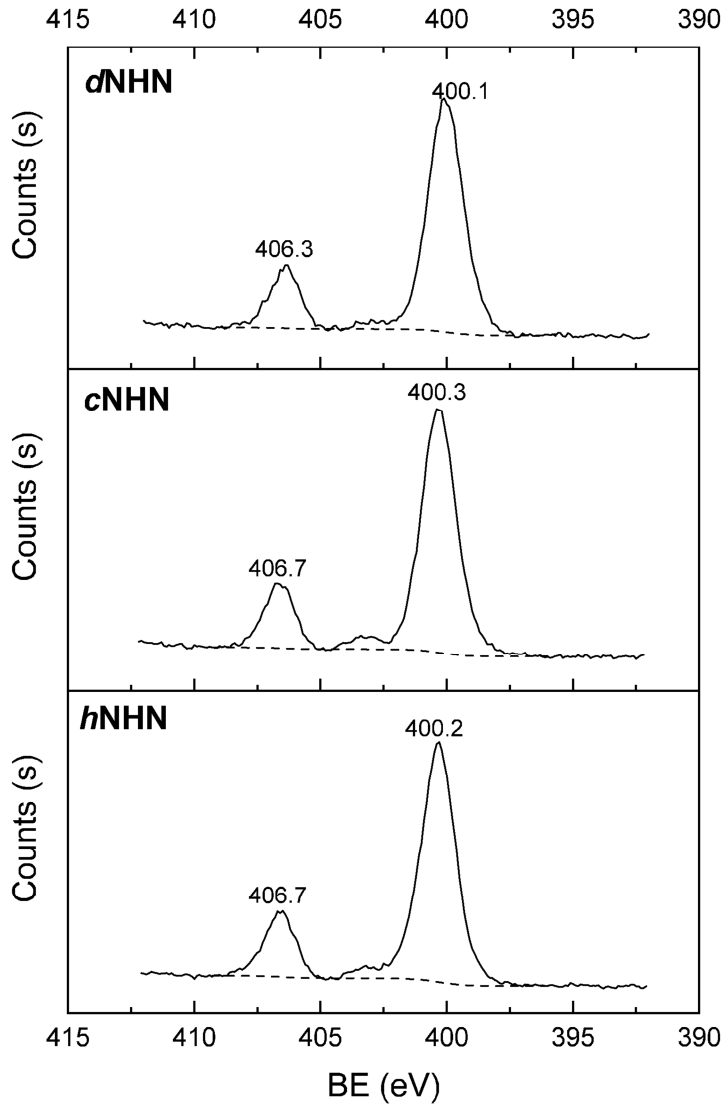

Figure 5. H_2 evolution curves obtained with ***h*NHN**, ***c*NHN** and ***d*NHN**. The hydrolysis conditions were as follows: 80°C; 11 mg of catalyst; 2 mL of alkaline water (0.5 NaOH); 100 mg $NaBH_4$.

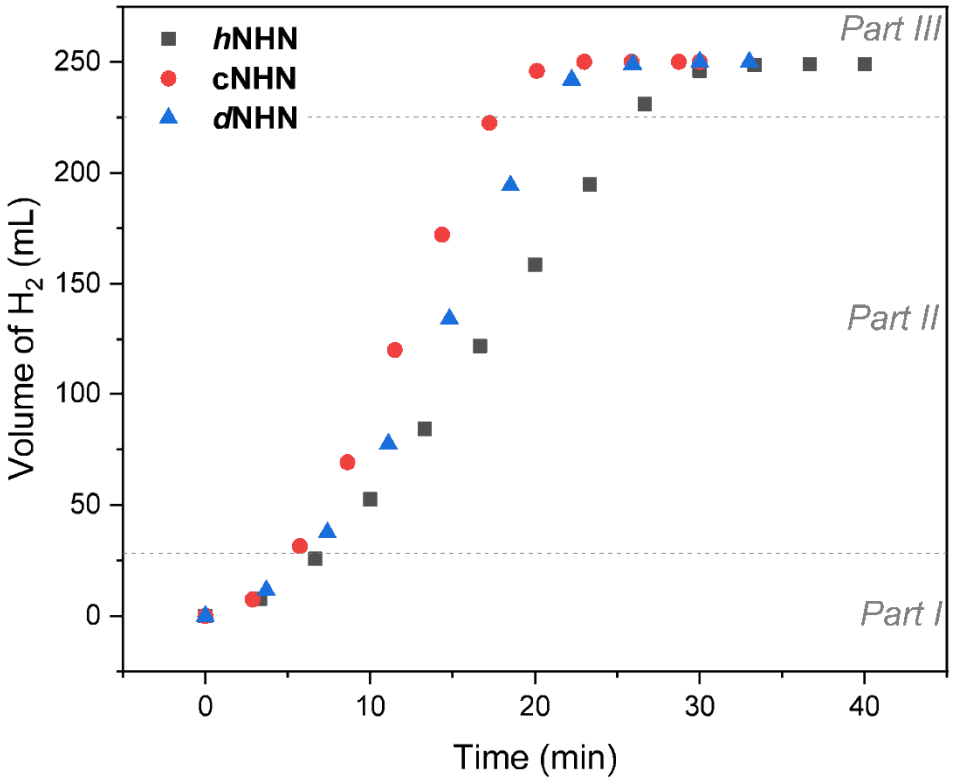

Figure 6. Analyses results of the spent fuel in either liquid-state (^{11}B NMR) or solid-state (^{11}B MAS NMR, FTIR and XRD). The chemical shifts of the NMR signals are given. The FTIR bands are ascribed to *e.g.* the B–O stretching and deformation modes. Some of the most intense XRD peaks are indexed (reference pattern 01-081-1512).

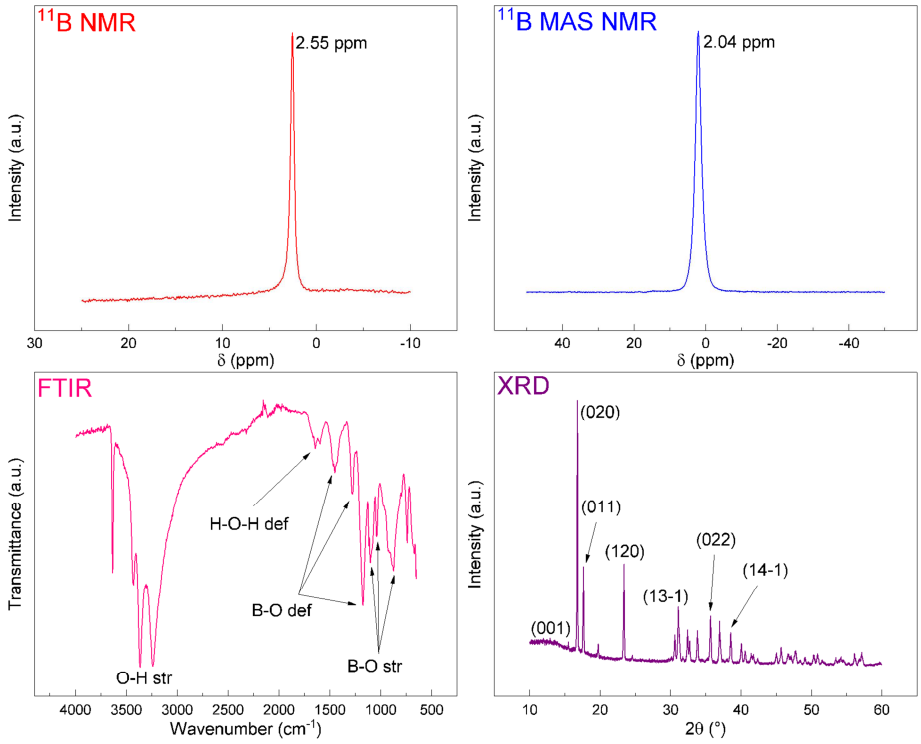

Figure 7. SEM images of the "reduced" nickel hydrazine nitrate complexes (recovered after the $NaBH_4$ hydrolysis experiments) denoted **R*h*NHN**, **R*c*NHN** and **R*d*NHN**.

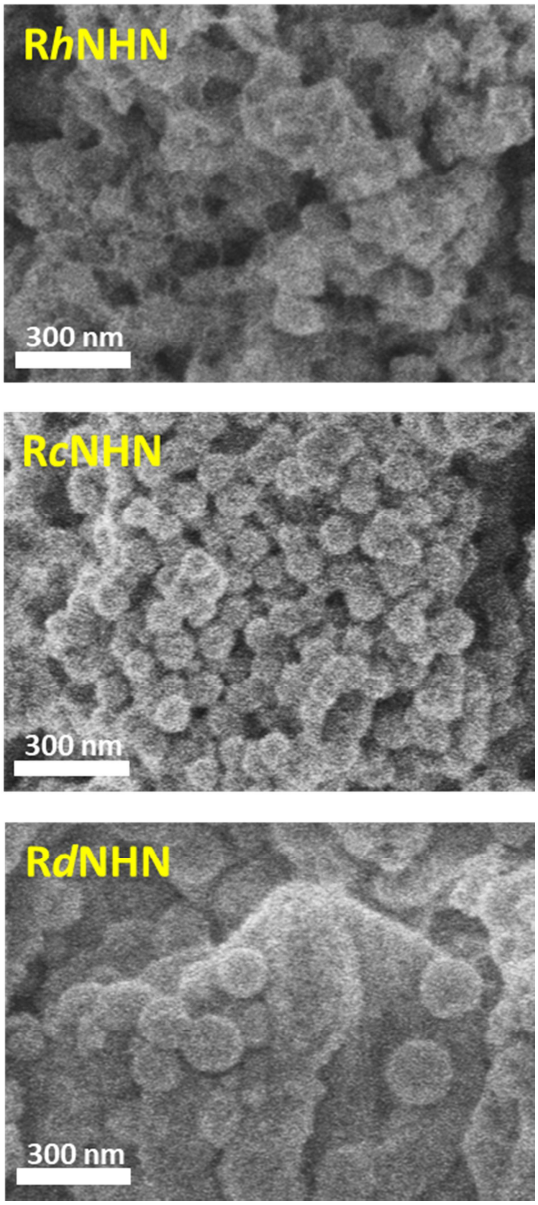

Figure 8. XPS spectra of the "reduced" nickel hydrazine nitrate complexes (recovered after the $NaBH_4$ hydrolysis experiments) denoted **R*h*NHN**, **R*c*NHN** and **R*d*NHN**: focus on the Ni 2p signals.

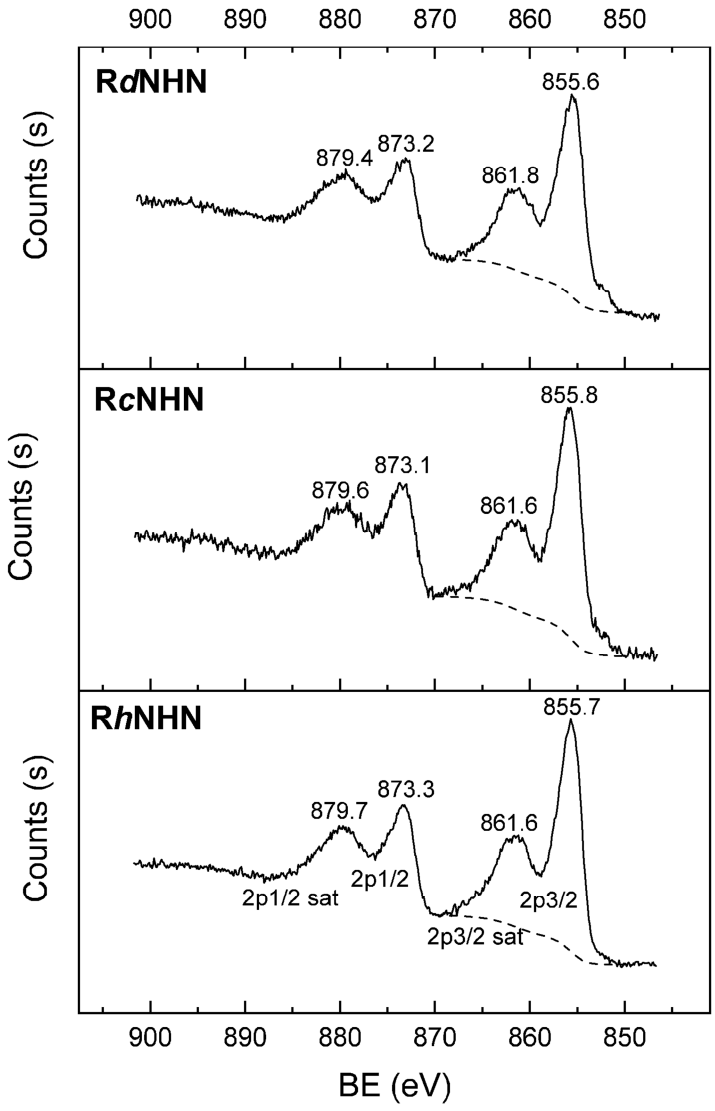

Figure 9. XPS spectra of the "reduced" nickel hydrazine nitrate complexes (recovered after the $NaBH_4$ hydrolysis experiments) denoted **R*h*NHN**, **R*c*NHN** and **R*d*NHN**: focus on the B 1s signals.

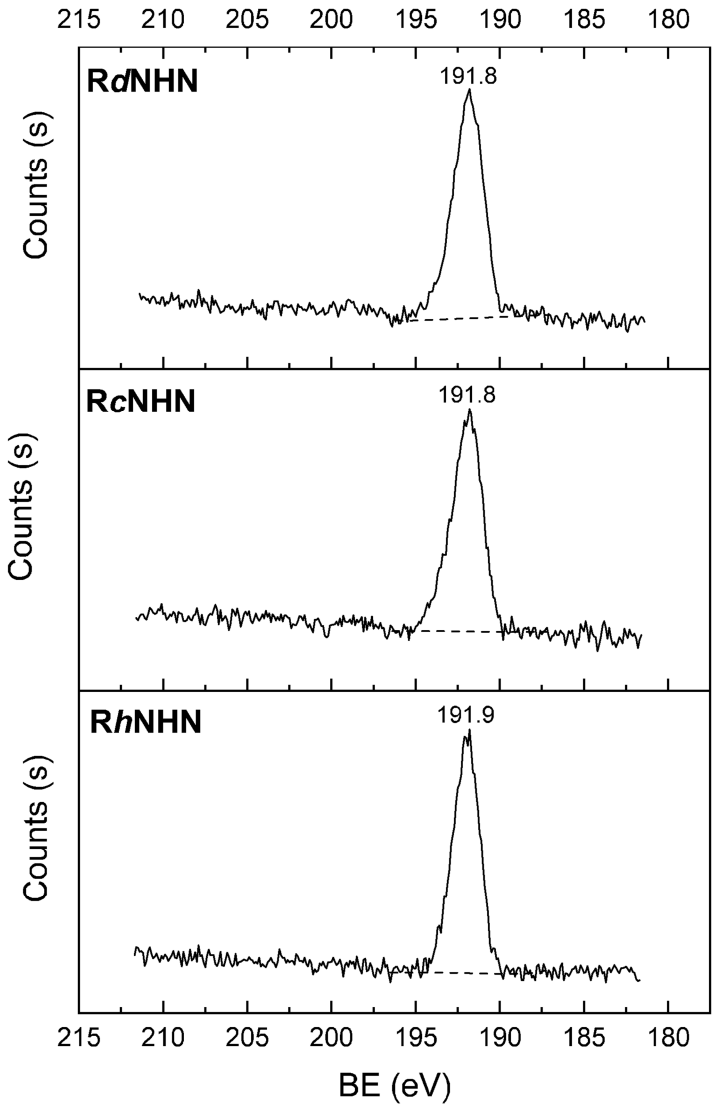

Figure 10. Comparison of the H_2 generation rates (denoted cycle 1) of **R*h*NHN**, **R*c*NHN** and **R*d*NHN** to the rates (denoted cycle 0) found with ***h*NHN**, ***c*NHN** and ***d*NHN**, and evolution of the H_2 generation rates of **R*h*NHN**, **R*c*NHN** and **R*d*NHN** over five cycles (cycle 1 to cycle 5; *i.e.* reusability experiments). The rates were calculated from the H_2 evolution curves shown in **Figures S20** to **S22**.

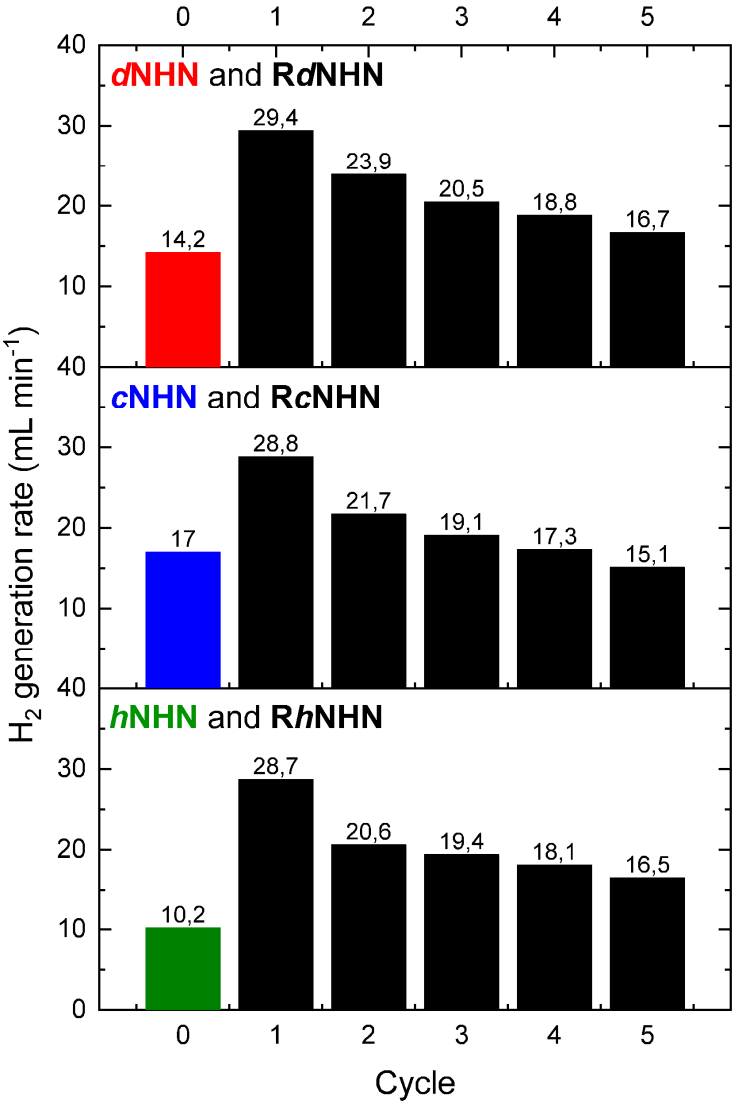

$NaBH_4 + 4H_2O$

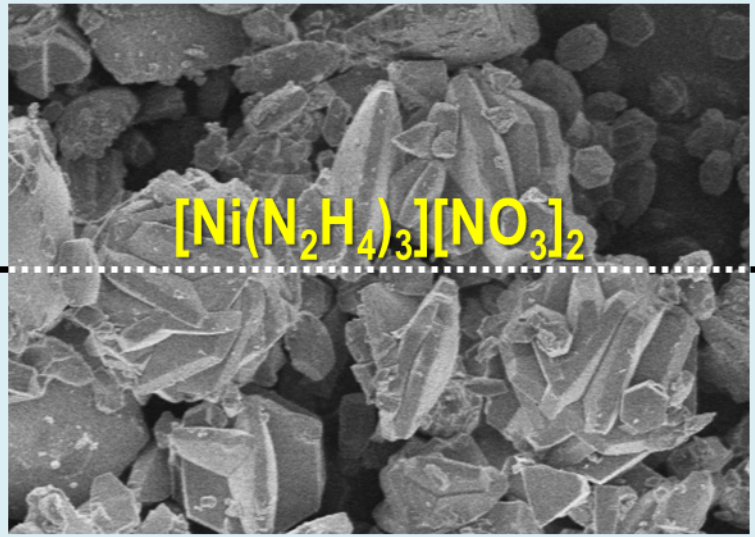

in situ

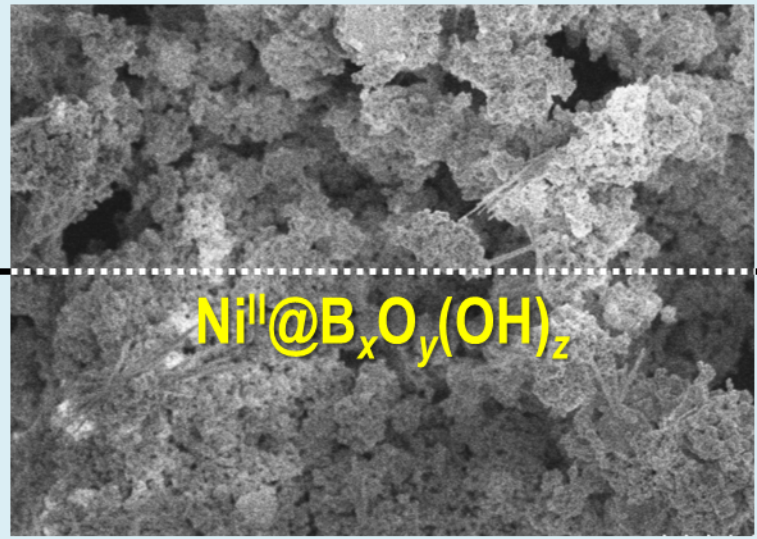

$NaB(OH)_4 + 4H_2$